ACS NANO

www.acsnano.org

ARTICLE

Flexible Carbon Nanotube Synaptic Transistor for Neurological Electronic Skin Applications

Haochuan Wan, Yunqi Cao, Li-Wei Lo, Junyi Zhao, Nelson Sepúlveda, and Chuan Wang*

Cite This: *ACS Nano* 2020, 14, 10402–10412

Read Online

ACCESS | Metrics & More | Article Recommendations | Supporting Information

ABSTRACT: There is an increasing interest in the development of memristive or artificial synaptic devices that emulate the neuronal activities for neuromorphic computing applications. While there have already been many reports on artificial synaptic transistors implemented on rigid substrates, the use of flexible devices could potentially enable an even broader range of applications. In this paper, we report artificial synaptic thin-film transistors built on an ultrathin flexible substrate using high carrier mobility semiconducting single-wall carbon nanotubes. The synaptic characteristics of the flexible synaptic transistor including long-term/short-term plasticity, spike-amplitude-dependent plasticity, spike-width-dependent plasticity, paired-pulse facilitation, and spike-time-dependent plasticity have all been systematically characterized. Furthermore, we have demonstrated a flexible neurological electronic skin and its peripheral nerve with a flexible ferroelectret nanogenerator (FENG) serving as the sensory mechanoreceptor that generates action potentials to be processed and transmitted by the artificial synapse. In such neurological electronic skin, the flexible FENG sensor converts the tactile input (magnitude and frequency of force) into presynaptic action potential pulses, which are then passed to the gate of the synaptic transistor to induce change in its postsynaptic current, mimicking the modulation of synaptic weight in a biological synapse. Our neurological electronic skin closely imitates the behavior of actual human skin, and it allows for instantaneous detection of force stimuli and offers biological synapse-like behavior to relay the stimulus signals to the next stage. The flexible sensory skin could potentially be used to interface with skeletal muscle fibers for applications in neuroprosthetic devices.

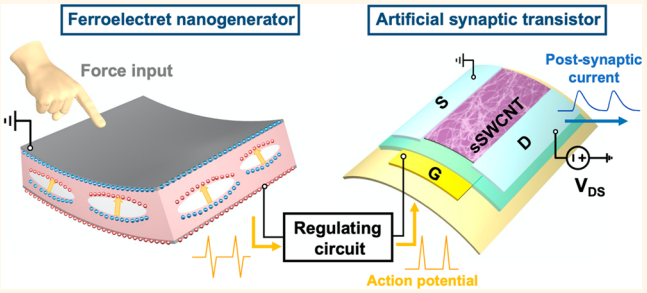

KEYWORDS: *electronic skin, carbon nanotube, flexible electronics, synaptic transistor, ferroelectret nanogenerator*

As the largest organ of the human body and the foundation of human physical interaction with the world, skin, with its complex tactile and thermal sensory capabilities, has intrigued and inspired enormous research efforts to mimic or even augment its functions. Artificial electronic skin (E-skin),[1−4] which was initially implemented primarily as a network of soft pressure sensors for spatial and temporal mapping of tactile information,[5−7] has recently been reinforced with a variety of additional sensing modalities and human-interactive functionalities, such as visualizable pressure detection,[8] *in situ* sweat analysis,[9] and haptic skin interfaces for virtual reality/augmented reality applications.[10] Previous studies of E-skin mainly utilize passive pressure-sensitive components such as resistive or capacitive pressure sensors to achieve physical−electrical signal transduction through their conductance or capacitance change.[5,11,12] In contrast, the signal transduction mechanism is more "active" in a biological skin system as sensory receptors embedded across the skin would directly transduce the physical contact into information-encoded, pulse-based electrical signals. On the other hand, neuronal functions (*i.e.*, the conveyance and transmission of such signals to the central nervous system (CNS) such as the brain and spinal cord) have not been explored in E-skin systems as extensively.

Signal communication between a sensory afferent neuron and a neuron in the CNS is enabled through a junction structure called a synapse. The strength of the synapse (synaptic weight) can be adjusted in response to the action potentials from sensory neurons, which is a crucial property that has been proven to be the foundation of mammal memory formation[13] and learning ability.[14] The modulation of synaptic weight can be emulated in electronic devices by modulating the channel conductance of two-terminal memristors or three-

Received: May 21, 2020
Accepted: July 17, 2020
Published: July 17, 2020

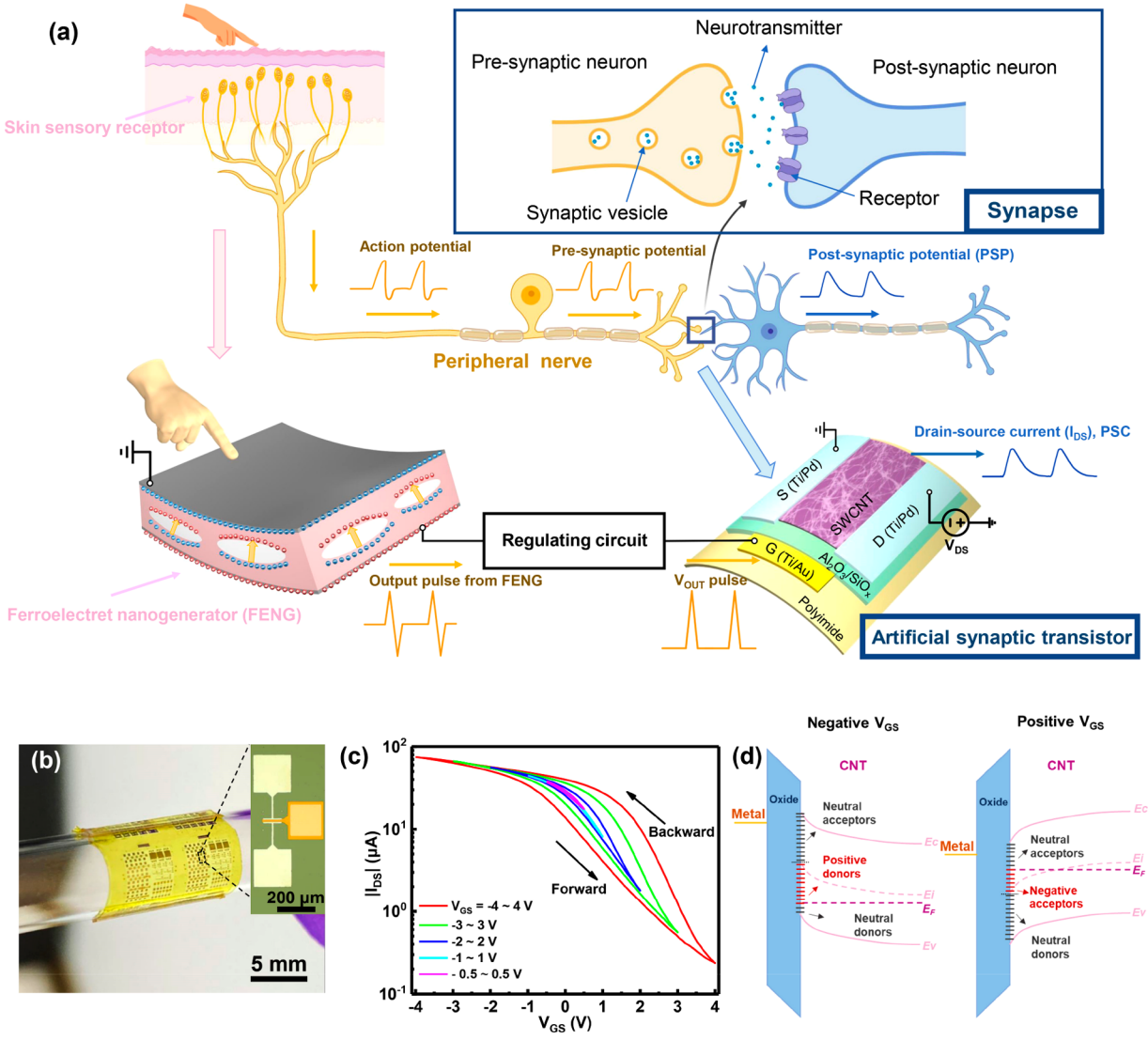

Figure 1. (a) Schematic illustration of biological skin, its peripheral nerve and synapse (upper part), in comparison with its artificial electrical counterpart (lower part). The schematic illustration is partially created with BioRender.com. (b) Optical photograph showing a sample of flexible carbon nanotube synaptic transistors. Inset: Optical micrograph of an individual synaptic transistor. (c) Double sweep transfer curves of the synaptic transistor showing the hysteresis under different V_{GS} sweeping ranges measured with $|V_{DS}| = 1.0$ V. (d) Energy band diagrams illustrating the origin of hysteresis induced by interface trap states under positive and negative gate biases in a sSWCNT synaptic transistor.

terminal artificial synaptic transistors.[15] As the action potential can be emulated by voltage pulse, the induced conductance change is usually presented in the form of a change in channel current, which is usually called postsynaptic current (PSC) in synaptic devices. Thanks to the recent development in flexible neuromorphic electronic materials and device technologies, it is now possible to achieve synaptic devices in flexible[16,17] or even stretchable forms[18,19] that can be compatible with soft and curved human skin or internal organs. Among the various neuromorphic electronic materials that have been studied, a one-dimensional (1D) semiconducting single-wall carbon nanotube (sSWCNT) offers an outstanding combination of mechanical robustness,[20,21] large on/off ratio, and high carrier mobility.[22,23] Owing to its 1D geometry and small physical size, the conductance of the sSWCNT is demonstrated to be highly sensitive to charged interface trap states,[24] allowing the sSWCNT-based artificial synaptic transistors to exhibit a broad conductance modulation range.[25] Interest and intrigue toward the sSWCNT in neuromorphic devices have been further expanded due to its established outstanding scalability and mechanical flexibility.[26−28] Wafer-scale aligned sSWCNT synaptic transistor arrays demonstrate exceptional device uniformity and repeatabilty,[29] whereas flexible sSWCNT synaptic transistors with extraordinary bendability on various flexible substrates[30,31] show a huge potential in wearable electronic applications.

In this study, we report a biomimetic electronic sensory skin by utilizing a flexible high-performance sSWCNT synaptic thin-film transistor to imitate the chemical synapse between a peripheral nerve and the CNS and thin-film ferroelectret nanogenerator (FENG) to imitate the mechanoreceptor and peripheral nerve itself for transducing and relaying the force stimulus information to the synapse. The illustration of the electronic system and the analogy to its biological counterpart is shown in Figure 1a. We have systematically studied the synaptic characteristics including long-term/short-term plasti-

https://dx.doi.org/10.1021/acsnano.0c04259
ACS Nano 2020, 14, 10402−10412

city (LTP/STP), spike-amplitude-dependent plasticity, spike-width-dependent plasticity, paired-pulse facilitation (PPF) and frequency filtering characteristics, analogue-synaptic weight-switching behavior with bending and cyclic tests, spike-time-dependent plasticity in the flexible sSWCNT synaptic transistor. The output characteristics of FENG in response to external force stimuli have also been studied. In the reported artificial sensory skin, the FENG sensor converts the tactile information (the force amplitude and frequency) of the physical contact into presynaptic action potential pulses, which are then passed to the gate of the synaptic transistor to render changes in drain current (PSC), mimicking the modulation of synaptic weight in a biological synapse. Such an operation of the synaptic transistor and its ability to maintain the change in conductance states allow the device to process the electrical signals from the sensor and generate history-dependent output that reflects not only the amplitude but also the sequence and frequency of the force stimuli. Our artificial sensory skin allows instantaneous sensing of force stimuli with biological synapse-like transmission, processing and memory of the stimulus signals. With the artificial synaptic transistor potentially interfacing with a motor or actuator unit, the sensory skin could have the potential for controlling skeletal muscle fibers or have applications in neuroprosthetic devices.

RESULTS AND DISCUSSION

Figure 1b shows a representative image of arrays of thin-film sSWCNT synaptic transistors fabricated on a flexible polyimide (PI) substrate being wrapped on a glass cylinder. The inset is an optical micrograph of an individual transistor with a channel length of L = 10 μm and a channel width of W = 100 μm. The transistor consists of Ti/Au back-gate electrode, Al_2O_3/SiO_x dielectric layer, a solution-processed sSWCNT active channel, and Ti/Pd source and drain electrodes. The microfabrication processes are described in the Methods section in detail. The transfer characteristics (family of $I_{DS}-V_{GS}$ curves) and output characteristics (family of $I_{DS}-V_{DS}$ curves) of the transistor are shown in Figure 1c and Supporting Information Figure S1, respectively. The output curves exhibit good saturation at different V_{GS} values from +4 to −4 V. From the transfer curve measured with V_{DS} = −1 V and V_{GS} sweeps from −4 to +4 V shown in Figure 1c, the device current on/off ratio (I_{on}/I_{off}) is 320 and the field-effect mobility is calculated to be 22.0 $cm^2\ V^{-1}\ s^{-1}$ using the equation $\mu = (L \cdot g_m)/(W \cdot C_G \cdot V_{DS})$, where V_{DS} = −1 V, g_m is the peak transconductance and C_G is the unit-area gate capacitance from our previous work.[20] Large I_{on}/I_{off} and high carrier mobility will ensure a large range for channel conductance change and thus good synaptic weight modulation,[29] which will be discussed later in the article. The high mobility of the sSWCNT thin-film transistors (TFTs) may also be beneficial in other neuromorphic applications, such as serving as logic circuits for a conventional memristor.[32]

Although the ideal CNT does not have surface dangling bonds, interface trap states still exist between the CNT and the oxide dielectric layer in a CNT transistor.[33,34] Figure 1d shows the energy band diagrams, illustrating the oxide/CNT interface states. When a negative gate bias is applied, the energy band of the CNT at the oxide/CNT interface and the interface states bend upward, while the Fermi level (E_F) of the CNT remains flat. In this scenario, more interface donor states become empty and positively charged, causing a negative shift of the corresponding $I_{DS}-V_{GS}$ curve and the threshold voltage (V_{th}). Similarly, when a positive gate bias is applied, the CNT energy band and interface states bend downward, causing more acceptor interface states to be filled and thus negatively charged, which leads to a positive shift of the $I_{DS}-V_{GS}$ curve and V_{th}. A nonlinear, hysteretic behavior of V_{th} from bidirectional V_{GS} sweeps (V_{GS} sweeping from negative to positive values, and *vice versa*) is observed. It is worth noting that the width of the hysteresis curve is directly associated with the range of V_{GS} sweeping. The value of hysteresis is generally defined as the difference between V_{GS} at average I_{DS}, that is, $(I_{DS\text{-}MAX} + I_{DS\text{-}MIN})/2$ from backward and forward sweeping curves. As shown in Figure 1c, when V_{GS} is swept from −4 to +4 V, a hysteresis of 1.44 V is observed. In contrast, if the sweeping range of V_{GS} is reduced to −0.5 to +0.5 V, the $I_{DS}-V_{GS}$ curve only exhibits negligible hysteresis. This phenomenon can be explained by the fact that greater V_{GS} biases result in more significant band bending in semiconductors, which allows a wider range of interface states to be charged and discharged. This increases the net interface charge density at the oxide/CNT interface, causing more significant shift in V_{th} and thus larger hysteresis.

In most logic circuit applications, hysteretic behavior in transistors is considered unfavorable and deemed to be eliminated.[35] However, hysteresis is also a distinctive property that enables memory, which could be harnessed and engineered for neuromorphic computing applications to mimic the behavior of the biological synapse in the human brain. In the human nervous system, a synapse is a gap-junction structure that enables the signal transmission between one neuron cell (presynaptic cell) to another neuron cell or an effector cell (postsynaptic cell) which can actively respond to a stimulus. How strongly the pre- and postsynaptic cells are correlated and can exert influence over each other is evaluated by the weight of the synapse, which can evolve over time and adjust to neuron activities. The adaptation of synaptic weight to the neuron stimulus (usually in the form of action potential) is known as synaptic plasticity. Based on how synaptic plasticity changes in response to different presynaptic action potentials, the synaptic weight can either be increased for an improved signal transmission between two cells through the synapse, decreased for a suppressed signal transmission, or simply remain unchanged. The aforementioned three basic synaptic plasticities are named potentiation, depression, and elasticity, respectively, and can all be imitated using the sSWCNT artificial synaptic transistors with hysteresis caused by interface states.

In a synaptic transistor, the gate terminal is used to imitate the presynaptic neuron, whereas the drain terminal is used to imitate the postsynaptic neuron. The synaptic weight is represented by I_{DS}, which is named postsynaptic current (PSC) in the synaptic transistor context. As explained previously, a negative gate bias will cause a negative shift of the $I_{DS}-V_{GS}$ curve while a positive bias will cause a positive one. When the gate bias is applied in the form of a pulse, the PSC in a synaptic transistor can be modified effectively. For example, a positive gate pulse with sufficient amplitude will result in an immediate increase in PSC (potentiation), whereas a negative gate pulse with sufficient amplitude will induce an immediate drop in PSC (depression). If the amplitude of gate bias is too small to generate noticeable hysteresis, the PSC is likely to remain constant. The amplitude of the action potential that leads to potentiation, depression, or elasticity may have slight variations among different devices, depending

https://dx.doi.org/10.1021/acsnano.0c04259
ACS Nano 2020, 14, 10402−10412

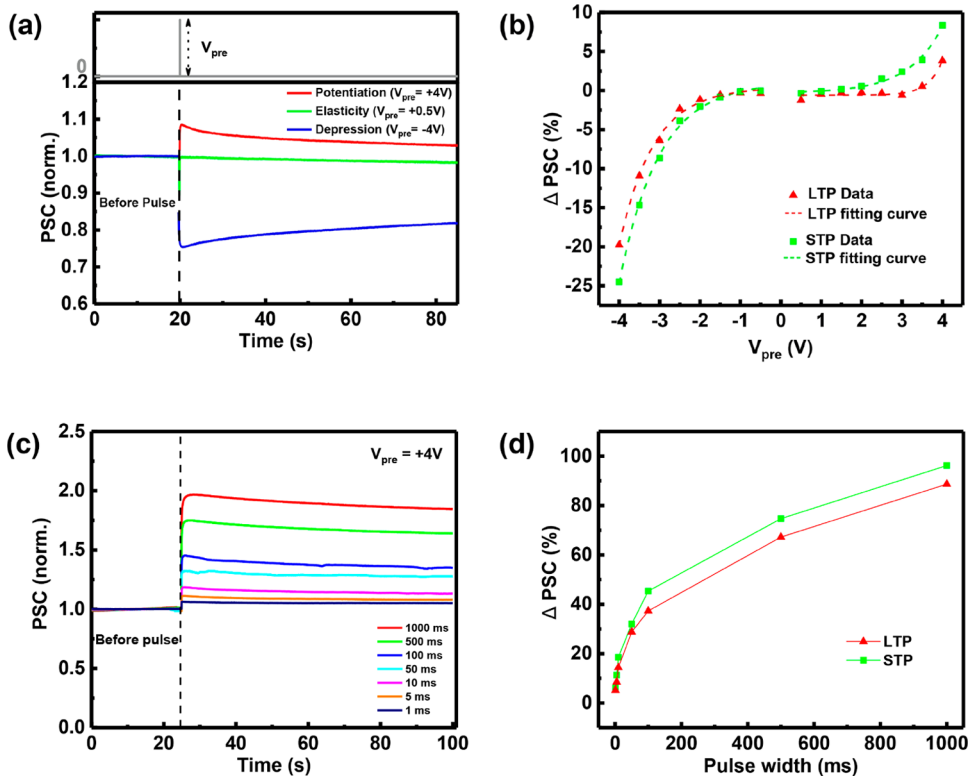

Figure 2. (a) Instantaneous PSC (normalized) before and after presynaptic pulse excitation showing potentiation (V_{pre} = +4 V), depression (V_{pre} = −4 V), and elasticity (V_{pre} = +0.5 V). (b) Spike-amplitude dependence of LTP and STP. (c) PSC responses of synaptic transistor with V_{pre} (+4 V) of different pulse widths ranging from 1 ms to 1 s. (d) Spike-width dependence of LTP and STP. All measurements are conducted at $|V_{DS}|$ = 1.0 V.

on the hysteresis curves of each individual transistor. Figure 2a shows the PSC response of the sSWCNT synaptic transistor to three representative presynaptic square wave action potentials (V_{pre}) with different amplitude of +4, +0.5, and −4 V, all with the same pulse width of 10 ms and baseline of 0 V. The $|V_{DS}|$ is fixed at 1 V during the measurement. The baseline value of the PSC is defined as the average PSC value between 5 and 15 s before the arrival of the V_{pre}, and the PSC data are normalized with respect to this baseline value. Upon arrival of the action potential, V_{pre} = +4 V yields a large increase in PSC, which can be interpreted as potentiation of the synaptic weight; V_{pre} = −4 V yields a large decrease in PSC corresponding to depression, and V_{pre} = +0.5 V gives elasticity with negligible change in PSC.

For synaptic weight modulation, aside from being stimulus-dependent, the time dependence is also crucial as human memory is believed to be the outcome of two types of temporal synaptic plasticity: short-term plasticity and long-term plasticity.[36] The STP has a time scale on the order of milliseconds to seconds, whereas the LTP is more long-lived and could last for minutes, hours, or even days. In our study, the STP is defined as the amount of percentage change in PSC (ΔPSC) after 1 s of the stimulation of V_{pre}, and LTP is defined as the average ΔPSC between 30 and 50 s after the stimulation. The spike-amplitude-dependent STP and LTP are plotted in Figure 2b as a function of the amplitude of V_{pre}, and the results can be well fitted with exponential function in the form of $\Delta PSC = \mp A_0 \exp\left(\frac{|V_{pre}|}{V_A}\right) + w_0$, where V_{pre} is the amplitude of the action potential, V_A is associated with the activation energy of the interface trap states and the "∓" sign indicates the type of plasticity.[37] The value of V_A determines how large the amplitude of V_{pre} needs to be to reach certain amount of STP/LTP. From the device structure point of view, V_A indicates how easily the interface donor/acceptor states can be charged. The smaller the value of V_A, the easier the synaptic transistor can be excited by V_{pre}, thus larger PSC change can be induced. For potentiation and depression, ΔPSC is positive and negative and the corresponding PSC is called excitatory PSC (EPSC) and inhibitory PSC (IPSC), respectively. The fitting equations of LTP and STP by potentiating V_{pre} and depressing V_{pre} are listed in Table S1 in the Supporting Information. It is believed that the amount of synaptic vesicles being activated and fusing with a presynaptic membrane to release a neurotransmitter depends on the amplitude of action potential.[37] In other words, the nature of biological synaptic weight modulation due to the quantitative change of released neurotransmitters is well-represented by the ΔPSC as a result of different magnitude of V_{pre} in the sSWCNT artificial synaptic transistor. To obtain a more comprehensive understanding of how a single action potential can affect the synaptic response of the transistor, action potentials with the same amplitude but different pulse widths are also applied to excite the transistor, and the corresponding PSC responses are measured. Figure 2c shows the PSC responses of a synaptic transistor with V_{pre} (+4 V) of various pulse widths ranging from 1 ms to 1 s. The spike-width dependences of STP and LTP are plotted in Figure 2d. Results in Figure 2c,d suggest a monotonic increase of synaptic response with the increased spike width, which can be attributed to the increased number of charged interface states due to the extended charging time.

https://dx.doi.org/10.1021/acsnano.0c04259
ACS Nano 2020, 14, 10402−10412

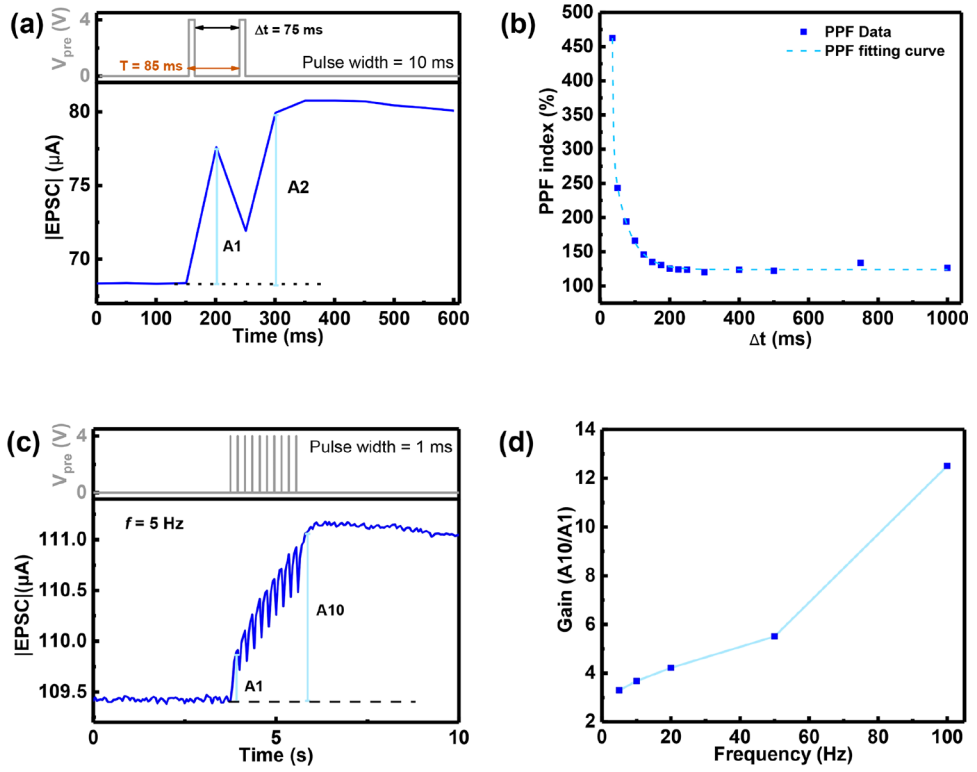

Figure 3. Short-term facilitation characteristics of the sSWCNT synaptic transistor. (a) Paired-pulse facilitation measurements showing EPSC change triggered by two consecutive pulses with a spike interval Δt of 75 ms. *A*1 and *A*2 are the height of the peaks in EPSC upon the arrival of the first pulse and the second pulse, respectively. (b) PPF index (defined as *A*2/*A*1 × 100%) plotted as a function of different spike intervals. (c) EPSC change triggered by a train of 10 pulses with a frequency of 5 Hz. *A*1 and *A*10 are the height of the peaks in EPSC upon the arrival of the first pulse and the last pulse, respectively. (d) Amplitude gain (defined as *A*10/*A*1 × 100%) plotted as a function of pulse train frequency showing the high-pass filtering characteristics of the synaptic transistor. All the measurements are conducted at $|V_{DS}|$ = 1.0 V.

From transistor structure and fabrication point of view, device geometry (*e.g.*, channel length *L*), type of dielectric material being deposited, deposition techniques of the dielectric layer, and the surface treatments of the dielectric layer can all affect the density and distribution of interface trap states, thus affecting the synaptic response of the transistor to V_{pre}. In order to understand the uniformity of the synaptic response, hysteresis curves and PSC curves of multiple devices are measured, and the results are shown in Supporting Information Figure S2. The synaptic transistors exhibit fairly uniform synaptic responses to the same V_{pre}, suggesting a good controllability over the interface trap states among different devices during the device fabrication processes. The variation of the synaptic behaviors can be attributed to the variation in hysteresis behaviors among transistors.

The synaptic behavior is further characterized by user-dependent synaptic plasticity—the change of synaptic weight with regards to the activation history at that synapse. For short-term plasticity, facilitation is one of the most common forms and plays an important role in synaptic computing and information processing.[38,39] Among the various facilitation forms, PPF is studied by applying a pair of stimuli to the presynapse neuron and monitoring the fractional change of a second response of the synaptic weight to the first one. The magnitude of this fractional change was demonstrated to be a function of the interval between the two action potentials.[40] In our sSWCNT synaptic transistor, the pair of stimuli are emulated by two consecutive presynaptic spikes to the gate of the transistor with an amplitude of +4 V, a width of 10 ms, and a period of 85 ms (*i.e.*, duty cycle of 11.76%). The "spike interval" Δt is defined as the time difference between the falling edge of the first spike and the rising edge of the second spike. For the aforementioned spike pair, a Δt of 75 ms is obtained and shown along with the spike pair in the upper panel of Figure 3a. It is noted that, for two consecutive pulses (*A*1 and *A*2, shown in bottom panel of Figure 3a), the EPSC response is higher for the second peak (*A*2). This behavior was repeatedly observed in multiple experiments and shows how past pulses can be used to increase future EPSC responses, which is indicative of memory behavior. Defined as the percentage of the amplitude of a second spike to the first spike in EPSC, the PPF index is used to evaluate the PPF effect and can vary as the Δt of the presynaptic spikes varies. Figure 3b shows the PPF index plotted as a function of Δt, and the plot yields a double exponential curve as the Δt increases from 35 to 1000 ms, indicating that the PPF behavior is characterized by two phases with different relaxation time constants. The obtained data can be fitted well by the equation PPF index = $C_1 \exp(-\Delta t/\tau_1) + C_2 \exp(-\Delta t/\tau_2) + C_0$,[16] where C_1 and C_2 are the maximum amounts of each facilitation phases and τ_1 and τ_2 are the time constants of the relaxation in each phase. The time constants τ_1 and τ_2 determine how fast the PPF index decays with the increase of spike interval Δt. The larger the value of τ_1 and τ_2, the slower the decay of PPF index would be. From the device structure point of view, τ_1 and τ_2 are also associated with the oxide/semiconductor interface trap states as they indicate how long the charges can retain in these trap states. Detailed fitting equation can be found in Table S1 in the

https://dx.doi.org/10.1021/acsnano.0c04259
ACS Nano 2020, 14, 10402−10412

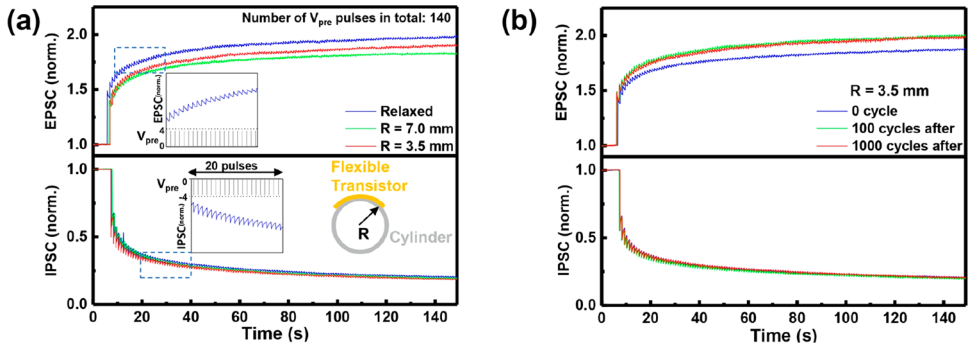

Figure 4. Synaptic weight modulation behavior and bending and cyclic tests of synaptic transistor. (a) Synaptic weight modulation curves of a synaptic transistor measured at various curvature radii. Inset: Zoomed-in view of a segment of the modulation curves with 20 cycles showing the detailed change of PSC under potentiating (top) and depressing (bottom) presynaptic action potentials. (b) Synaptic weight modulation curves after various numbers of bending cycles at curvature radius of 3.5 mm. All measurements are conducted at $|V_{DS}|$ = 1.0 V.

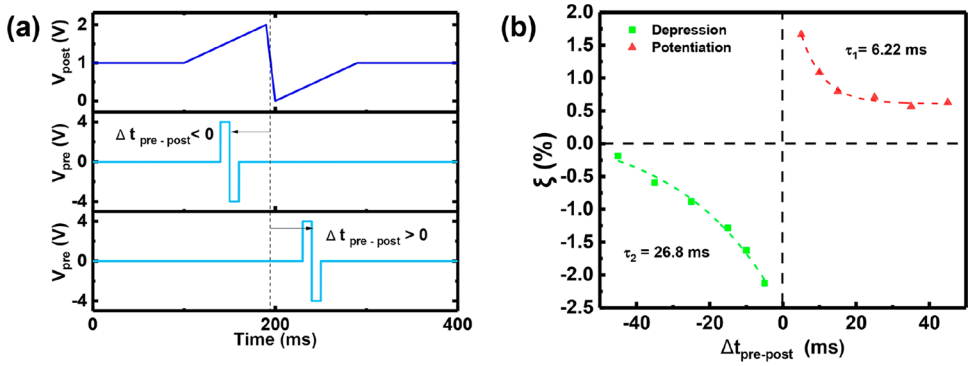

Figure 5. Spike-time-dependent plasticity of synaptic transistor. (a) Waveforms of postsynaptic spike and presynaptic spike. (b) Plots of parameter ζ (same value as LTP) of synaptic transistor as a function of different presynaptic and postsynaptic time interval values ($\Delta t_{pre-post}$). Result shows a typical anti-Hebbian STDP behavior.

Supporting Information. Compared with biological synapse with $\tau_1 \approx 50$ ms and $\tau_2 \approx 300$ ms,[41] our artificial sSWCNT synaptic transistor resembles its biological counterpart with similar PPF behavior.

The facilitation behavior of STP was studied further beyond PPF in information processing function of a synapse. For example, when an animal travels through different locations in a particular environment, certain regions in its hippocampus would fire sequences of spike discharges to the synapses to be processed.[42] The frequency of this train of spikes, usually containing spatial information, can vary and induce different animal behaviors, indicating filtering characteristics of the synapse. In our study, a train of spikes comprising 10 pulses with a width of 1 ms, an amplitude of +4 V, and frequencies ranging from 5 to 100 Hz are applied to the artificial synaptic transistor (Figure 3c). The EPSC yields a peak once a pulse from the train arrives, and the amplitude gain of the EPSC is defined as the ratio of the height of the peak after the tenth pulse ($A10$) and the height of the peak after the first pulse ($A1$), expressed as $A10/A1$. Figure 3d shows the gain of EPSC plotted as a function of the spike train frequency, and the result shows that the amplitude gain increases from 3.3 to 12.5 as the frequency increases from 5 to 100 Hz, suggesting the high-pass filtering behavior of our artificial synaptic transistor. This result is in good accordance with simulations reported in the literature showing elevated synaptic strength (weight) with increasing stimulus frequency.[42]

The ability of the synapse to gradually modulate its synaptic weight by periodic spikes from presynaptic neurons can be emulated by the channel conductance-switching behavior of the artificial synaptic transistor, where the conductance of the channel can be discretely adjusted by the presynaptic pulses and thus exhibit different analogue states.[25,29] With $|V_{DS}|$ fixed at 1 V, the value of the channel conductance, $G = I_{DS}/V_{DS}$, is equal to PSC, thus the modulation of the conductance could be represented by the EPSC and IPSC change. The potentiation and depression conductance modulation tests are carried out by applying a train of 140 presynaptic spikes with a pulse width of 10 ms, a pulse period of 1 s, and a pulse amplitude of +4 V for potentiation or −4 V for depression. Because of the outstanding mechanical robustness of sSWCNT and the very thin (∼10 μm) polyimide substrate used, the sSWCNT synaptic transistors are expected to exhibit good flexibility, and thus bendability and endurance of the synaptic transistors are also examined in this measurement. Figure 4a shows the potentiation and depression conductance modulations under different bending conditions. In a relaxed state, the range of the total potentiation conductance modulation after 140 pulses is measured to be 98.9%

$$\left(\frac{\text{EPSCmax} - \text{EPSCmin}}{\text{EPSCmin}} \times 100\%\right)$$

and total depression conductance modulation is measured to be −80.3%

$$\left(-\frac{\text{IPSCmax} - \text{IPSCmin}}{\text{IPSCmin}} \times 100\%\right)$$

https://dx.doi.org/10.1021/acsnano.0c04259
ACS Nano 2020, 14, 10402−10412

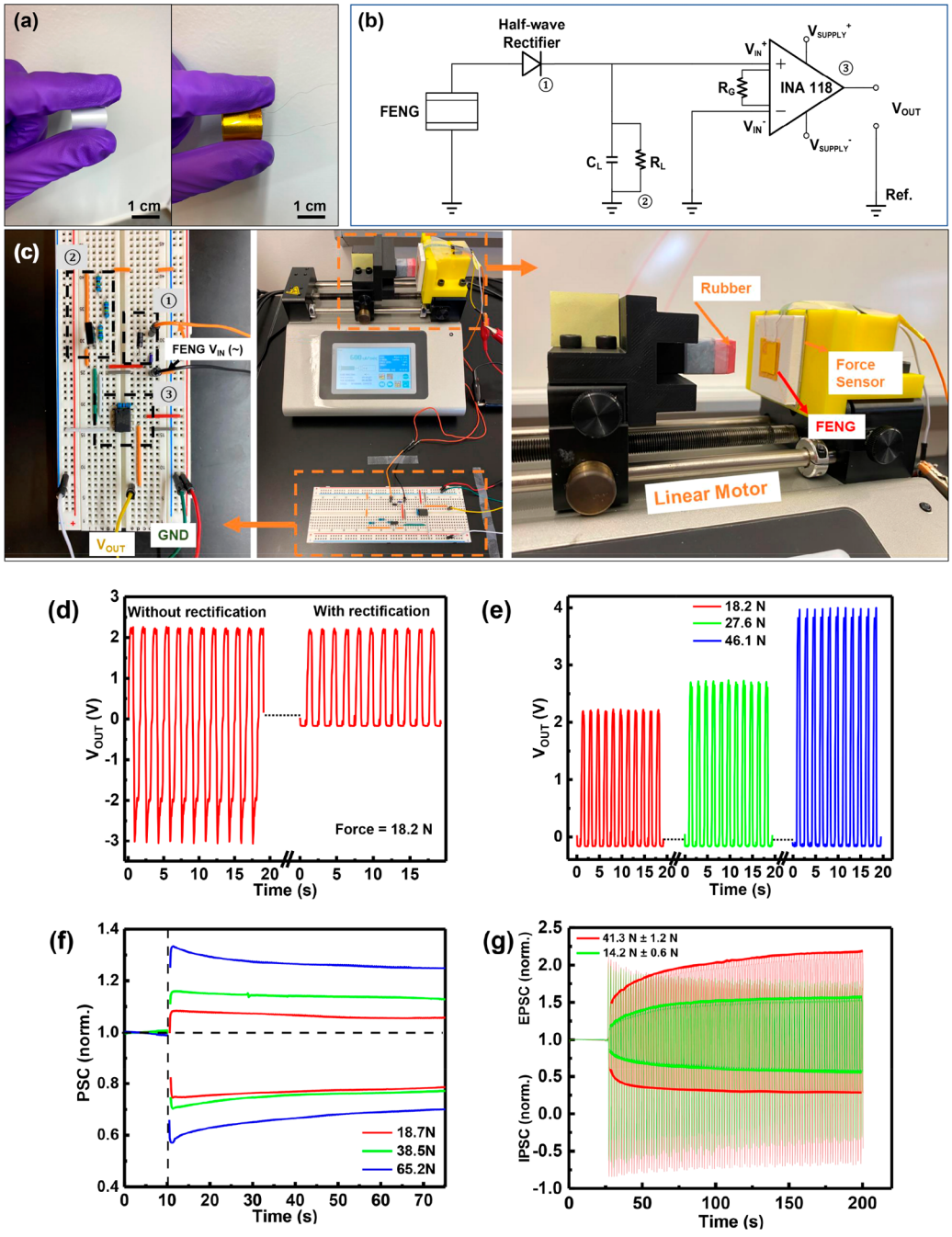

Figure 6. Artificial electronic sensory skin with the mechanoreceptor implemented by a FENG and its peripheral nerve implemented by a sSWCNT synaptic transistor. (a) Photograph of a 1.2 × 1.2 cm^2 flexible FENG film. Left: Pristine PPFE film. Right: Complete FENG device with sputtered silver electrodes and PI encapsulation. (b) Schematic of FENG and the regulating circuit. (c) Photograph of the actual regulating circuit (major components marked in numbers with respect to circuit diagram in (b)) and the mechanical loading test setup. (d) Output signal V_{OUT} with and without half-wave rectification. (e) Rectified output signal V_{OUT} under different loading forces. (f) Instantaneous PSC change (normalized) of a synaptic transistor under different loading forces. (g) Synaptic weight modulation curves measured with periodical loading forces of 41.3 or 14.2 N at a frequency of 0.67 Hz. Solid lines: Peak values of EPSC or IPSC. Background: Measured raw EPSC and IPSC data. All synaptic behavior measurements are conducted at $|V_{DS}|$ = 1.0 V.

The inset images in Figure 4a reveal the detailed view of the conductance tuning by 20 applied pulses with each small "step" of the postsynaptic current (the value of EPSC or IPSC 1 s after the arrival of a pulse), representing a discrete analogue channel conductance state. Compared with traditional cross-bar-structured memristor with limited dynamic range of conductance modulation,[43] the large tuning range of channel conductance of our synaptic transistor could enhance the efficiency of neuromorphic computing when the device is implemented in the artificial neural system.[25,30] For the flexibility tests, the modulation curves of the device in Figure 4a exhibit only slight variations under potentiation and negligible changes under depression when the sample is bent down to a curvature radii of 7.5 mm and 3.5 mm, respectively. The modulation curves exhibit similar behavior under cyclic bending tests when the sample is repeatedly bent to a

https://dx.doi.org/10.1021/acsnano.0c04259
ACS Nano 2020, 14, 10402−10412

curvature radius of 3.5 mm for up to 1000 cycles, as shown in Figure 4b. The results demonstrate the outstanding mechanical flexibility and robustness of the sSWCNT synaptic transistor and thus capacitate the device for applications in soft wearable electronic systems.

In a biological synapse, the synaptic weight responds not only to the action potential from a presynaptic neuron but also to the reflected postsynaptic action potential when the signal is passing through the axon of the postsynaptic neuron.[44] When the time correlation of pre- and postsynaptic spikes follows certain learning rules, a specific long-term plasticity known as spike-timing-dependent plasticity (STDP) arises and is regarded as a fundamental process to understand the activity-dependent development in the human brain.[15] In Figure 5a, the postsynaptic spike is emulated by a ramped wave with a period of 190 ms being applied to the drain terminal of the synaptic transistor. The postsynaptic spike starts at a baseline of +1 V, linearly ramping up to +2 V in 90 ms, decreasing to 0 V in 10 ms, and ramping up again to the baseline of +1 V in 90 ms. The presynaptic spikes are two 10 ms square waves adjacent to each other and with opposite polarities (amplitude = +4 V for the first square wave and −4 V for the second square wave). As shown in Figure 5a, the timeline midpoint of the pre- and postsynaptic spike is defined as t_{pre} and t_{post}, and the spike time difference, $\Delta t_{pre\text{-}post} = t_{pre} - t_{post}$, is used as an indicator of the arrival time sequence of pre- and postsynaptic spikes. A negative $\Delta t_{pre\text{-}post}$ indicates the arrival of presynaptic spike precedes the postsynaptic spike, and a positive $\Delta t_{pre\text{-}post}$ indicates the arrival of a presynaptic spike succeeds the postsynaptic spike. The parameter ζ, which is defined as the LTP value of the synaptic transistor after the activation by both the pre- and postsynaptic spikes, is adapted to characterize the STDP behavior of the device. Figure 5b shows the data of ζ plotted as a function of $\Delta t_{pre\text{-}post}$; the results indicate that positive $\Delta t_{pre\text{-}post}$ generates potentiation in the synaptic transistor, whereas negative $\Delta t_{pre\text{-}post}$ generates depression. For both potentiation and depression, when the arrival time of the pre- and postsynaptic spike are more correlated (*i.e.*, smaller absolute value of $\Delta t_{pre\text{-}post}$), greater change in synaptic weight is observed. The measured STDP data can also be fitted with exponential functions, and the time constants are extracted to be 6.22 ms for potentiation and 26.8 ms for depression (see Table S1 in the Supporting Information for detailed fitting equations). The results exhibit a typical anti-Hebbian STDP form[15] and may be utilized in neuromorphic networks for learning and pattern recognition.[25]

In the human nervous system, the tactile information is picked up by the mechanoreceptors that reside in human skin and passed through the axon of its peripheral nerve in the form of action potential. The action potential containing the information is relayed to the CNS, which then signals other neuron cells or body parts to execute appropriate responses. Flexible tactile transducers such as triboelectric nanogenerator[45] or ferroelectret nanogenerator[46] can be readily used to convert external force stimulus to a pulsed electrical signal without the need for a power supply, and they exhibit behaviors that closely resemble skin mechanoreceptors. In this study, a flexible polypropylene-based FENG device reported in our previous work is used as the tactile transducer due to its high efficiency and biocompatibility, as shown in Figure 6a.[47] A mechanical input (displacement, force, pressure) generates dipole moments across polypropylene's thickness, creating an electric field that is compensated by the accumulation of charge of opposite polarities at both surfaces of the material. This charge can be collected through thin metal film contacts on the polymer surface, resulting in a small electrical current that is proportional to the rate of change in the applied mechanical input, and flows in opposite directions depending on the direction of the input cycle (*e.g.*, compression/relaxation). This unregulated electrical output pulse from the FENG needs to be regulated using the rectifying and amplifying circuits illustrated in Figure 5b. In brief, the pulsed current signal from FENG is first rectified by a p−n junction diode, which serves as a half-wave rectifier to remove the negative component. The rectified current signal will subsequently charge the capacitor in a RC circuit, creating an initial voltage V_0 across that capacitor. Following the zero-input response equation of a first-order RC circuit, the responsive voltage across the capacitor can be written as $v(t) = V_0 \times \exp(-t/\tau_T)$, $t \geq 0$, which decays exponentially with time constant $\tau_T = R_L C_L$. When the discharged capacitor is recharged by subsequent current pulses, $v(t)$ will increase exponentially to V_0 with the same τ_T. In this study a τ_T of 30 ms is set, producing a theoretical rise/fall time of 66 ms (2.2 τ_T) of the voltage pulse. It is worth noting that while the rise and fall time of the voltage pulse are mainly controlled by τ_T, the period and duty cycle of that pulse are primarily controlled by the period of the applied force to the FENG. The pulsed voltage signal from RC circuit is then sent to the positive input terminal (V_{IN}^+) of an instrumentation amplifier (TI INA118) and the output of which is amplified as $V_{OUT} = G(V_{IN}^+ - V_{IN}^-)$, where G is the voltage gain and $G = (50\ k\Omega/R_G) + 1$. The R_G value in the present work of 10 kΩ results in a theoretical voltage gain of 6. The amplified pulsed voltage output (V_{OUT}) from the amplifier is then sent to the gate terminal of the sSWCNT synaptic transistor as the presynaptic action potential. This signal processing circuit avoids the impedance mismatch between the FENG and synaptic transistor and allows the tuning of the action potential pulse through altering the period of loading force, time constant of RC circuit, and gain of the amplifier. In Figure 5c, the actual implementation of a rectifying and amplifying circuit is displayed on the left side, and the mechanical loading test setup used for generating pulses in the FENG device is shown on the right side. The loading force is exerted by a rubber piston with a contact area of 1.2 × 1.2 cm^2 mounted on a horizontal-moving linear motor (Legato 110 syringe pump, kd Scientific), and a PI-encapsulated FENG device (1.2 × 1.2 cm^2, same area as piston head) is mounted on the stationary scaffold with a commercial force sensor (FSR01CE, Ohmite) placed behind the nanogenerator to precisely monitor the magnitude and frequency of the applied forces by the motor. During the measurement, the rubber piston is carefully aligned with the thin-film FENG and pushed toward the device with preset moving distance. Both the V_{OUT} and the force sensor resistance are measured by a semiconductor device analyzer (Keysight B1500A). The detailed force measurement information can be found in Figure S3 in the Supporting Information. Figure 5d shows the V_{OUT} signal with and without the rectification, and the rectified V_{OUT} signal will be subsequently used as presynaptic action potential pulse for the synaptic transistor. The data show that a train of rectified positive pulses with an average amplitude of 2.2 V, a period of 1.68 s, and a duty cycle of 56.5% is generated with a loading force of 18.2 N and a frequency of 0.67 Hz. Additionally, the amplitude of V_{OUT} increases monotonically with increasing

https://dx.doi.org/10.1021/acsnano.0c04259
ACS Nano 2020, 14, 10402−10412

loading force, as shown in Figure 5e. The average amplitude of the signal increases from 2.2 to 4.0 V as the applied force increases from 18.2 to 46.1 N with the same frequency. A small negative voltage drift (~150 mV) of the V_{OUT} signal is observed due to the input offset voltage of the instrumentation amplifier (driven by dual voltage supply of −15 and +15 V). This voltage drift can potentially be reduced using a high-quality amplifier with better precision in our future study. It is also worth mentioning that the polarity of the pulse can be readily inverted by interchanging the input terminals from V_{IN}^{+} to V_{IN}^{-} in the amplifier, which allows both potentiation and depression to be achieved in the synaptic transistor.

Finally, the integration of the flexible FENG device with a flexible sSWCNT synaptic transistor to emulate the behavior of a neurological electronic skin is demonstrated. Figure 5f shows the instantaneous synaptic weight modulation of the artificial synaptic transistor by the force-encoded presynaptic action potentials. For short-term potentiation and depression, the synaptic weight changes under a force stimulus of 18.7 or 65.2 N are +8.44 or +32.62% and −25.15 or −41.17%, respectively. Similarly, for long-term potentiation and depression, the synaptic weight changes under force stimulus of 18.7 or 65.2 N are +6.07 or +26.05% and −22.60 or −32.10%, respectively. The data are normalized to the baseline PSC, which is defined as the average PSC from 0 to 5 s. The results above show that an increased magnitude of the force stimulus perceived by FENG is transduced into greater change in PSC and thus greater modification of synaptic weight. The history-dependent, discrete modulation of synaptic weight under continuous stimulation has also been studied, and the results are presented in Figure 5g. Trains of 100 potentiating and depressing action potential pulses with a frequency of 0.67 Hz are generated by stimulating the FENG with forces of 41.2 or 14.2 N and relayed to the synaptic transistor to be processed. In Figure 5g, the peak values of PSC change to each potentiation or depression pulse are sorted out and connected by a solid line to show the trend of synaptic weight modification, with the real-time actual responses of PSC also shown in the background. The synaptic weight responses of the transistor show gradual analogue modulation of the synaptic weight similar to what is shown in Figure 4. After 100 action potential spikes from the FENG, a total synaptic weight modification of +118.9 or +56.5% for potentiation at 41.3(±1.2) or 14.2(±0.6) N and −72.1 or −44.3% for depression at 41.3(±1.2) or 14.2(±0.6) N can be observed. The variation in the loading force is due to the slight movement of the supporting scaffold during the continuous measurement. Successfully reproducing analogue-like synaptic weight modulation with force-encoded information further demonstrates the feasibility of interfacing a FENG-driven circuit with a sSWCNT synaptic transistor as a sensory electronic skin and nerve. This is a step toward the use of flexible electronic devices for neuroprosthetics applications.

CONCLUSION

In summary, we have demonstrated a biomimicking sensory electronic skin system whose neurological function of biological synapse is realized by a flexible sSWCNT artificial synaptic transistor. Temporal synaptic behaviors such as STP and LTP have been demonstrated with potentiating, depressing, or elastic action potentials at different amplitudes, widths, and polarities. Short-term and history-dependent nature of the synaptic transistor is elaborated by PPF, high-pass filtering characteristics, and synaptic weight modulation behavior, whereas long-term learning and memory ability of the transistor is represented by the STDP. The sensory function of the electronic skin is achieved using a FENG as the sensor, which directly generates pulsed electrical signals or action potentials in response to force stimulus. By integrating a synaptic transistor with the sensory component of the electronic skin, tactile information containing the magnitude and activating history of the force stimuli is successfully transduced and relayed to the presynaptic terminal of the synaptic transistor and then processed and transmitted in the form of change in synaptic weight. By interfacing with motor units of animal or human bodies in the future, our sensory electronic skin can have the potential of facilitating the advancement of wearable neuromorphic applications such as an artificial nerve system or smart medical prosthetics.

METHODS

Fabrication of a Flexible Carbon Nanotube Synaptic Transistor. Polyimide from HD Microsystems is spin-coated (1000 rpm, 30 s; 2000 rpm, 1 min) onto a Si/SiO_2 wafer and baked on a hot plate at 300 °C for 10 min to form a uniform PI thin film with a thickness of around 10 μm. On top of the PI substrate, a Ti/Au (5/30 nm) bottom-gate electrode is formed by photolithography and lift-off, followed by dielectric layer deposition of Al_2O_3/SiO_x (20/15 nm) using atomic layer deposition and e-beam evaporation. Before the CNT channel material deposition, poly-L-lysine solution (0.1% w/v; Sigma-Aldrich) is used to functionalize the dielectric layer surface to improve the adhesion of the CNT and thus increase the CNT network uniformity. After functionalization, the sample is rinsed with DI water and immersed into the as-purchased sSWCNT solution (0.01 mg/mL, NanoIntegris Inc.) for 15 min to deposit active channel material. The sample is then taken out and rinsed with DI water and isopropyl alcohol, blow-dried by N_2, and annealed in a vacuum oven at 200 °C for 1 h to evaporate the residues. After that, Ti/Pd (0.5/35 nm) source and drain electrodes are formed by photolithography and e-beam evaporation, and as a final step, the transistor is finalized by etching away the sSWCNT outside the source−drain-defined channel region using oxygen plasma.

Fabrication of a Flexible Ferroelectret Nanogenerator. Two sides of a purchased PPFE (Emfit Corporation) thin film (80 μm) are sputter-coated with Ag electrodes of 500 nm (Hummer X, Anatech Inc.). A sample with an area of 1.2 × 1.2 cm^2 is prepared, and each side of the sample is connected to a copper wire *via* copper tape. The device is then encapsulated by two polyimide films (20 μm, Kapton) as protection layers.

Electrical Measurements. All electrical data are measured using a Keysight B1500A semiconductor device analyzer. Except for the pulses that are generated from the FENG in Figure 6, all other pulse signals are generated by a Keysight 33510B waveform generator.

ASSOCIATED CONTENT

Supporting Information

The Supporting Information is available free of charge at https://pubs.acs.org/doi/10.1021/acsnano.0c04259.

Equations for fitting the curves of synaptic behavior measurements (S1), output curves of the sSWCNT synaptic transistor (S2), device uniformity (S3), and force measurement using a commercial force sensor (S4) (PDF)

AUTHOR INFORMATION

Corresponding Author

Chuan Wang − *Electrical and Systems Engineering and Institute of Materials Science and Engineering, Washington University in*

https://dx.doi.org/10.1021/acsnano.0c04259
ACS Nano 2020, 14, 10402−10412

St. Louis, St. Louis, Missouri 63130, United States; orcid.org/0000-0002-5296-0631; Email: chuanwang@wustl.edu

Authors

Haochuan Wan − *Electrical and Systems Engineering, Washington University in St. Louis, St. Louis, Missouri 63130, United States*

Yunqi Cao − *Electrical and Computer Engineering, Michigan State University, East Lansing, Michigan 48824, United States*

Li-Wei Lo − *Electrical and Systems Engineering and Institute of Materials Science and Engineering, Washington University in St. Louis, St. Louis, Missouri 63130, United States*

Junyi Zhao − *Electrical and Systems Engineering, Washington University in St. Louis, St. Louis, Missouri 63130, United States*

Nelson Sepúlveda − *Electrical and Computer Engineering, Michigan State University, East Lansing, Michigan 48824, United States;* orcid.org/0000-0002-9676-8529

Complete contact information is available at: https://pubs.acs.org/10.1021/acsnano.0c04259

Notes

The authors declare no competing financial interest.

ACKNOWLEDGMENTS

This work was partially funded by a Michigan State University Foundation Strategic Partnership Grant (No. 16-SPG-Full-3236). The authors acknowledge the financial support from Washington University in St. Louis and the Institute of Materials Science and Engineering for the use of instruments and staff assistance.

REFERENCES

(1) Hammock, M. L.; Chortos, A.; Tee, B. C. K.; Tok, J. B. H.; Bao, Z. 25th Anniversary Article: The Evolution of Electronic Skin (E-Skin): A Brief History, Design Considerations, and Recent Progress. *Adv. Mater.* **2013**, *25*, 5997−6038.

(2) Chortos, A.; Liu, J.; Bao, Z. Pursuing Prosthetic Electronic Skin. *Nat. Mater.* **2016**, *15*, 937−950.

(3) Rogers, J. A.; Someya, T.; Huang, Y. Materials and Mechanics for Stretchable Electronics. *Science* **2010**, *327*, 1603−1607.

(4) Takei, K.; Gao, W.; Wang, C.; Javey, A. Physical and Chemical Sensing with Electronic Skin. *Proc. IEEE* **2019**, *107*, 2155−2167.

(5) Takei, K.; Takahashi, T.; Ho, J. C.; Ko, H.; Gillies, A. G.; Leu, P. W.; Fearing, R. S.; Javey, A. Nanowire Active-Matrix Circuitry for Low-Voltage Macroscale Artificial Skin. *Nat. Mater.* **2010**, *9*, 821−826.

(6) Someya, T.; Sekitani, T.; Iba, S.; Kato, Y.; Kawaguchi, H.; Sakurai, T. A Large-Area, Flexible Pressure Sensor Matrix with Organic Field-Effect Transistors for Artificial Skin Applications. *Proc. Natl. Acad. Sci. U. S. A.* **2004**, *101*, 9966−9970.

(7) Someya, T.; Kato, Y.; Sekitani, T.; Iba, S.; Noguchi, Y.; Murase, Y.; Kawaguchi, H.; Sakurai, T. Conformable, Flexible, Large-Area Networks of Pressure and Thermal Sensors with Organic Transistor Active Matrixes. *Proc. Natl. Acad. Sci. U. S. A.* **2005**, *102*, 12321−12325.

(8) Wang, C.; Hwang, D.; Yu, Z.; Takei, K.; Park, J.; Chen, T.; Ma, B.; Javey, A. User-Interactive Electronic Skin for Instantaneous Pressure Visualization. *Nat. Mater.* **2013**, *12*, 899−904.

(9) Gao, W.; Emaminejad, S.; Nyein, H. Y. Y.; Challa, S.; Chen, K.; Peck, A.; Fahad, H. M.; Ota, H.; Shiraki, H.; Kiriya, D.; Lien, D.-H.; Brooks, G. A.; Davis, R. W.; Javey, A. Fully Integrated Wearable Sensor Arrays for Multiplexed *In Situ* Perspiration Analysis. *Nature* **2016**, *529*, 509−514.

(10) Yu, X.; Xie, Z.; Yu, Y.; Lee, J.; Vazquez-Guardado, A.; Luan, H.; Ruban, J.; Ning, X.; Akhtar, A.; Li, D.; Ji, B.; Liu, Y.; Sun, R.; Cao, J.; Huo, Q.; Zhong, Y.; Lee, C.; Kim, S.; Gutruf, P.; Zhang, C.; Xue, Y.; Guo, Q.; Chempakasseril, A.; Tian, P.; Lu, W.; Jeong, J.; Yu, Y.; Cornman, J.; Tan, C.; Kim, B.; Lee, K.; Feng, X.; Huang, Y.; Rogers, J. A. Skin-Integrated Wireless Haptic Interfaces for Virtual and Augmented Reality. *Nature* **2019**, *575*, 473−479.

(11) Kim, Y.; Chortos, A.; Xu, W.; Liu, Y.; Oh, J. Y.; Son, D.; Kang, J.; Foudeh, A. M.; Zhu, C.; Lee, Y.; Niu, S.; Liu, J.; Pfattner, R.; Bao, Z.; Lee, T.-W. A Bioinspired Flexible Organic Artificial Afferent Nerve. *Science* **2018**, *360*, 998−1003.

(12) Mannsfeld, S. C.; Tee, B. C.; Stoltenberg, R. M.; Chen, C. V. H.; Barman, S.; Muir, B. V.; Sokolov, A. N.; Reese, C.; Bao, Z. Highly Sensitive Flexible Pressure Sensors with Microstructured Rubber Dielectric Layers. *Nat. Mater.* **2010**, *9*, 859−864.

(13) Kleim, J. A.; Freeman, J. H.; Bruneau, R.; Nolan, B. C.; Cooper, N. R.; Zook, A.; Walters, D. Synapse Formation Is Associated with Memory Storage in the Cerebellum. *Proc. Natl. Acad. Sci. U. S. A.* **2002**, *99*, 13228−13231.

(14) Gruart, A.; Muñoz, M. D.; Delgado-García, J. M. Involvement of the Ca3-Ca1 Synapse in the Acquisition of Associative Learning in Behaving Mice. *J. Neurosci.* **2006**, *26*, 1077−1087.

(15) Park, H. L.; Lee, Y.; Kim, N.; Seo, D. G.; Go, G. T.; Lee, T. W. Flexible Neuromorphic Electronics for Computing, Soft Robotics, and Neuroprosthetics. *Adv. Mater.* **2020**, *32*, 1903558.

(16) Liu, Q.; Liu, Y.; Li, J.; Lau, C.; Wu, F.; Zhang, A.; Li, Z.; Chen, M.; Fu, H.; Draper, J.; Cao, X.; Zhou, C. Fully Printed All-Solid-State Organic Flexible Artificial Synapse for Neuromorphic Computing. *ACS Appl. Mater. Interfaces* **2019**, *11*, 16749−16757.

(17) van de Burgt, Y.; Lubberman, E.; Fuller, E. J.; Keene, S. T.; Faria, G. C.; Agarwal, S.; Marinella, M. J.; Talin, A. A.; Salleo, A. A Non-Volatile Organic Electrochemical Device as a Low-Voltage Artificial Synapse for Neuromorphic Computing. *Nat. Mater.* **2017**, *16*, 414−418.

(18) Shim, H.; Sim, K.; Ershad, F.; Yang, P.; Thukral, A.; Rao, Z.; Kim, H.-J.; Liu, Y.; Wang, X.; Gu, G.; Gao, L.; Wang, X.; Chai, Y.; Yu, C. Stretchable Elastic Synaptic Transistors for Neurologically Integrated Soft Engineering Systems. *Sci. Adv.* **2019**, *5*, No. eaax4961.

(19) Molina-Lopez, F.; Gao, T. Z.; Kraft, U.; Zhu, C.; Ohlund, T.; Pfattner, R.; Feig, V. R.; Kim, Y.; Wang, S.; Yun, Y.; Bao, Z. Inkjet-Printed Stretchable and Low Voltage Synaptic Transistor Array. *Nat. Commun.* **2019**, *10*, 1−10.

(20) Wang, C.; Chien, J.-C.; Takei, K.; Takahashi, T.; Nah, J.; Niknejad, A. M.; Javey, A. Extremely Bendable, High-Performance Integrated Circuits Using Semiconducting Carbon Nanotube Networks for Digital, Analog, and Radio-Frequency Applications. *Nano Lett.* **2012**, *12*, 1527−1533.

(21) Cao, X.; Cao, Y.; Zhou, C. Imperceptible and Ultraflexible *p*-Type Transistors and Macroelectronics Based on Carbon Nanotubes. *ACS Nano* **2016**, *10*, 199−206.

(22) Cao, Q.; Kim, H.-s.; Pimparkar, N.; Kulkarni, J. P.; Wang, C.; Shim, M.; Roy, K.; Alam, M. A.; Rogers, J. A. Medium-Scale Carbon Nanotube Thin-Film Integrated Circuits on Flexible Plastic Substrates. *Nature* **2008**, *454*, 495−500.

(23) Sun, D. M.; Liu, C.; Ren, W. C.; Cheng, H. M. A Review of Carbon Nanotube-and Graphene-Based Flexible Thin-Film Transistors. *Small* **2013**, *9*, 1188−1205.

(24) Bushmaker, A. W.; Oklejas, V.; Walker, D.; Hopkins, A. R.; Chen, J.; Cronin, S. B. Single-Ion Adsorption and Switching in Carbon Nanotubes. *Nat. Commun.* **2016**, *7*, 10475.

(25) Kim, S.; Yoon, J.; Kim, H.-D.; Choi, S.-J. Carbon Nanotube Synaptic Transistor Network for Pattern Recognition. *ACS Appl. Mater. Interfaces* **2015**, *7*, 25479−25486.

(26) Wang, C.; Zhang, J.; Ryu, K.; Badmaev, A.; De Arco, L. G.; Zhou, C. Wafer-Scale Fabrication of Separated Carbon Nanotube Thin-Film Transistors for Display Applications. *Nano Lett.* **2009**, *9*, 4285−4291.

(27) Cao, X.; Lau, C.; Liu, Y.; Wu, F.; Gui, H.; Liu, Q.; Ma, Y.; Wan, H.; Amer, M. R.; Zhou, C. Fully Screen-Printed, Large-Area, and Flexible Active-Matrix Electrochromic Displays Using Carbon Nanotube Thin-Film Transistors. *ACS Nano* **2016**, *10*, 9816−9822.

(28) Yu, M.; Wan, H.; Cai, L.; Miao, J.; Zhang, S.; Wang, C. Fully Printed Flexible Dual-Gate Carbon Nanotube Thin-Film Transistors with Tunable Ambipolar Characteristics for Complementary Logic Circuits. *ACS Nano* **2018**, *12*, 11572−11578.
(29) Sanchez Esqueda, I.; Yan, X.; Rutherglen, C.; Kane, A.; Cain, T.; Marsh, P.; Liu, Q.; Galatsis, K.; Wang, H.; Zhou, C. Aligned Carbon Nanotube Synaptic Transistors for Large-Scale Neuromorphic Computing. *ACS Nano* **2018**, *12*, 7352−7361.
(30) Kim, S.; Choi, B.; Lim, M.; Yoon, J.; Lee, J.; Kim, H.-D.; Choi, S.-J. Pattern Recognition Using Carbon Nanotube Synaptic Transistors with an Adjustable Weight Update Protocol. *ACS Nano* **2017**, *11*, 2814−2822.
(31) Yang, K.; Yuan, S.; Huan, Y.; Wang, J.; Tu, L.; Xu, J.; Zou, Z.; Zhan, Y.; Zheng, L.; Seoane, F. Tunable Flexible Artificial Synapses: A New Path toward a Wearable Electronic System. *npj Flexible Electron.* **2018**, *2*, 20.
(32) Sangwan, V. K.; Hersam, M. C. Neuromorphic Nanoelectronic Materials. *Nat. Nanotechnol.* **2020**, *15*, 517.
(33) Park, R. S.; Shulaker, M. M.; Hills, G.; Suriyasena Liyanage, L.; Lee, S.; Tang, A.; Mitra, S.; Wong, H.-S. P. Hysteresis in Carbon Nanotube Transistors: Measurement and Analysis of Trap Density, Energy Level, and Spatial Distribution. *ACS Nano* **2016**, *10*, 4599−4608.
(34) Lee, J. S.; Ryu, S.; Yoo, K.; Choi, I. S.; Yun, W. S.; Kim, J. Origin of Gate Hysteresis in Carbon Nanotube Field-Effect Transistors. *J. Phys. Chem. C* **2007**, *111*, 12504−12507.
(35) Kim, W.; Javey, A.; Vermesh, O.; Wang, Q.; Li, Y.; Dai, H. Hysteresis Caused by Water Molecules in Carbon Nanotube Field-Effect Transistors. *Nano Lett.* **2003**, *3*, 193−198.
(36) Ohno, T.; Hasegawa, T.; Tsuruoka, T.; Terabe, K.; Gimzewski, J. K.; Aono, M. Short-Term Plasticity and Long-Term Potentiation Mimicked in Single Inorganic Synapses. *Nat. Mater.* **2011**, *10*, 591−595.
(37) Arnold, A. J.; Razavieh, A.; Nasr, J. R.; Schulman, D. S.; Eichfeld, C. M.; Das, S. Mimicking Neurotransmitter Release in Chemical Synapses *Via* Hysteresis Engineering in Mos2 Transistors. *ACS Nano* **2017**, *11*, 3110−3118.
(38) Abbott, L.; Regehr, W. G. Synaptic Computation. *Nature* **2004**, *431*, 796−803.
(39) Zucker, R. S.; Regehr, W. G. Short-Term Synaptic Plasticity. *Annu. Rev. Physiol.* **2002**, *64*, 355−405.
(40) Regehr, W. G. Short-Term Presynaptic Plasticity. *Cold Spring Harbor Perspect. Biol.* **2012**, *4*, No. a005702.
(41) Johnston, D.; Wu, S. M.-S. *Foundations of Cellular Neurophysiology*; The MIT Press: Cambridge, MA, 1994; pp 309−313.
(42) Klyachko, V. A.; Stevens, C. F. Excitatory and Feed-Forward Inhibitory Hippocampal Synapses Work Synergistically as an Adaptive Filter of Natural Spike Trains. *PLoS Biol.* **2006**, *4*, e207.
(43) Jo, S. H.; Chang, T.; Ebong, I.; Bhadviya, B. B.; Mazumder, P.; Lu, W. Nanoscale Memristor Device as Synapse in Neuromorphic Systems. *Nano Lett.* **2010**, *10*, 1297−1301.
(44) Sarkar, D.; Tao, J.; Wang, W.; Lin, Q.; Yeung, M.; Ren, C.; Kapadia, R. Mimicking Biological Synaptic Functionality with an Indium Phosphide Synaptic Device on Silicon for Scalable Neuromorphic Computing. *ACS Nano* **2018**, *12*, 1656−1663.
(45) Fan, F.-R.; Tian, Z.-Q.; Wang, Z. L. Flexible Triboelectric Generator. *Nano Energy* **2012**, *1*, 328−334.
(46) Li, W.; Torres, D.; Wang, T.; Wang, C.; Sepúlveda, N. Flexible and Biocompatible Polypropylene Ferroelectret Nanogenerator (Feng): On the Path toward Wearable Devices Powered by Human Motion. *Nano Energy* **2016**, *30*, 649−657.
(47) Cao, Y.; Figueroa, J.; Pastrana, J. J.; Li, W.; Chen, Z.; Wang, Z. L.; Sepúlveda, N. Flexible Ferroelectret Polymer for Self-Powering Devices and Energy Storage Systems. *ACS Appl. Mater. Interfaces* **2019**, *11*, 17400−17409.

https://dx.doi.org/10.1021/acsnano.0c04259
ACS Nano 2020, 14, 10402−10412